Manuel Utecht | Tillmann Klamroth

Local resonances in STM manipulation of chlorobenzene on Si(111)-7×7

performance of different cluster models and density functionals

Suggested citation referring to the original publication:
Molecular Physics 116 (2018) 13, pp. 1687–1696
DOI http://dx.doi.org/10.1080/00268976.2018.1442939
ISSN (print) 0026-8976
ISSN (online) 1362-3028

MOLECULAR PHYSICS, 2018
VOL. 116, NO. 13, 1687–1696
https://doi.org/10.1080/00268976.2018.1442939

Taylor & Francis
Taylor & Francis Group

RESEARCH ARTICLE

OPEN ACCESS Check for updates

Local resonances in STM manipulation of chlorobenzene on Si(111)-7×7: performance of different cluster models and density functionals

Manuel Utecht and Tillmann Klamroth

Institut für Chemie, Universität Potsdam, Potsdam-Golm, Germany

ABSTRACT

Hot localised charge carriers on the Si(111)-7×7 surface are modelled by small charged clusters. Such resonances induce non-local desorption, i.e. more than 10 nm away from the injection site, of chlorobenzene in scanning tunnelling microscope experiments. We used such a cluster model to characterise resonance localisation and vibrational activation for positive and negative resonances recently. In this work, we investigate to which extent the model depends on details of the used cluster or quantum chemistry methods and try to identify the smallest possible cluster suitable for a description of the neutral surface and the ion resonances. Furthermore, a detailed analysis for different chemisorption orientations is performed. While some properties, as estimates of the resonance energy or absolute values for atomic changes, show such a dependency, the main findings are very robust with respect to changes in the model and/or the chemisorption geometry.

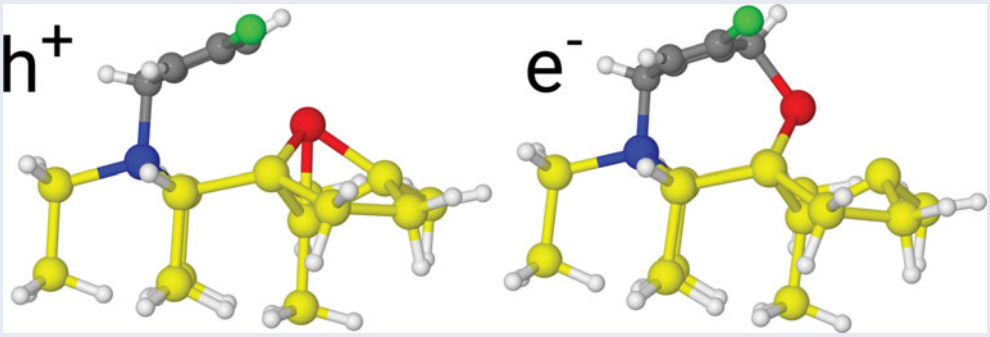

ARTICLE HISTORY
Received 15 December 2017
Accepted 14 February 2018

KEYWORDS
DFT; cluster model; charge localisation; STM

1. Introduction

The manipulation of single molecules or atoms using scanning tunnelling microscopes (STMs)[1–4] represents the lower size limit of nanotechnology. Such experiments not only point to numerous possible applications in information technology, they can be also regarded as model systems for reactions induced by low energy charge carriers, i.e. electrons or holes, at surfaces or interfaces. These processes and their in-depth understanding are of great importance for a broad range of diverse research fields, like photo-catalytic water splitting [5] or cancer research, e.g. the breaking of DNA strands [6]. Therefore, a lot of elementary reaction steps like dissociation [7], desorption [8], bond formation [9] and the switching of molecules [10–12] between metastable states have been studied with and induced by STM.

In such STM experiments, the reactions are often caused by inelastic electron tunnelling (IET). Other possible causes are the electric field in the tunnelling junction or purely mechanical interactions. For the IET case, the electrons can either couple to permanent dipole moments of the adsorbate [13] or transiently occupy empty electronic states at the adsorbate, so-called negative or positive ion resonances [14]. For these processes many dynamical simulations have been performed, which mostly employ either one nuclear potential energy surface (PES) for dipole couplings and ion resonances in the below threshold limit [13–16] or a few (mostly two) representative PES for the above threshold case [17–19]. Such models have already been widely used in the field of surface photochemistry for the desorption induced by electronic transitions [20] or desorption induced by multiple electronic transitions [21].

CONTACT Manuel Utecht manuel.utecht@uni-potsdam.de

Desorption and dissociation of chlorobenzene from/at the Si(111)-7×7 surface are well studied model processes for electron-induced reactions on surfaces. Both, STM-induced desorption [22] and dissociation [23] of the carbon-chlorine-bond, have been reported in experiments at room temperature. Desorption can be induced by electrons or holes (positive or negative bias voltage) and was found to be largely non-local [8,24]. We characterised physisorbed and chemisorbed chlorobenzene using a cluster approach and density functional theory (DFT) in Ref. [25]. These calculations used a di-σ bonded structure involving adjacent adatoms and rest-atoms on the Si(111)-7×7 surface as reported in Ref. [26] based on high resolution electron energy loss spectroscopy data and previous STM experiments [27] (see Ref. [25] and references therein for details about the different adsorption sites in the 7×7 unit cell). The calculated adsorption energies were ≈ 1.6 eV (chemisorption) and 0.6 eV (physisorption). While the physisorption energy agreed quite well with the experiment at that time (see Ref. [7] and references therein), the chemisorption energy seemed to be too high compared to 1.0 eV derived from thermal desorption spectra [26] assuming first-order kinetics and a pre-exponential factor of 10^{13} s^{-1}. Also, periodic DFT calculations [22] using a 2×2 mimic surface reported 1.2 eV chemisorption energy. However, new time-lapse STM experiments [28] indicate that the used pre-factor is too small and result in a chemisorption energy of ≈1.4 eV, well in line with our cluster calculations.

The non-local electron-induced desorption and surface diffusion of chlorobenzene, toluene and benzene was investigated by STM-experiments in Ref. [29]. This one electron process was found to be largely independent on the injection bias and the specific benzene derivate in a range from ≈2.0 to ≈2.8 eV, with a threshold voltage of 1.4 eV. The authors recorded the reaction probabilities as a function of the distance to the injection side and the surface temperature. In these experiments, no dependence of the reaction probability on the azimuthal angle and an increased charge transport range for higher surface temperatures are found. Both findings indicate that the underlying transport is not ballistic. Furthermore, the distance and temperature dependence could be successfully modelled by a surface charge diffusion model.

The hole-driven process for toluene on Si(111)-7×7 was investigated in Ref. [30]. Here, two thresholds at -1.2 and -1.5 eV were identified. In addition to the diffusive hole transport, a region near to the injection site (<15 nm) was identified where a ballistic hole transport leads to a substantial reduction of the reaction probability, which one would expect from a purely diffusive model. Furthermore, it was demonstrated that the hole-induced desorption is connected to a surface silicon adatom excitation [31]. For the thermally activated electron-induced desorption of chlorobenzene in Ref. [32], a low-temperature thermal activation energy of (21 ± 4) meV was determined. A refined analysis and new experiments [33] yield low-temperature activation energies of (13 ± 3) meV for electrons and (60 ± 10) meV for holes in the non-local desorption.

In summary, these experiments indicate that a large part of the STM-induced desorption/diffusion reactions of benzene derivates on Si(111)-7×7 is initiated by 'hot' localised charge carriers above a certain threshold energy diffusing at the surface region. For such carriers we introduced a cluster model in Ref. [34]. There, a small cluster was used, which mimics a localised, hot charge carrier simply by setting the total charge to either +1 or -1 in a quantum chemical calculation. In this way we avoid the calculation of excited charged states of the extended surface, which would have to be put in a coherent superposition, in order to describe a localised, hot charge carrier in an extended periodic system.

However, cluster models are known to depend often substantially on the details of the model, especially the potential energy landscape for silicon clusters is known to be very flat (see, e.g. [35]). Therefore, slightly different boundaries or different adsorption geometries could lead to large changes in the results. Also, the localisation or delocalisation of excess charges can be quite different depending on the functional used, e.g. GGA (generalised gradient approximation) type functionals or hybrid functionals (see, for instance [36]).

Therefore, the purpose of this paper is *(1)* to demonstrate that the findings of our cluster approach are fairly independent of details of the clusters and quantum chemistry methods used and (2) to perform a further in-depth analysis of the found resonances. Another focus is to identify the smallest cluster able to describe the ion resonances and the neutral surface. This cluster can be used in further investigations for Born–Oppenheimer molecular dynamics simulations, in order to clarify the details of the desorption processes. In addition, we want to analyse the influence of different adsorption geometries on the resonances and the charge localisation. Therefore, we compare a smaller cluster (**A**) to the one used in Ref. [34] (**B**) and compare results of different density functionals (see below).

2. Model and methods

2.1. Cluster models

The Si(111)-7×7-surface can be described by a centrosymmetric unit cell. Here, we start, as in Refs. [25,34],

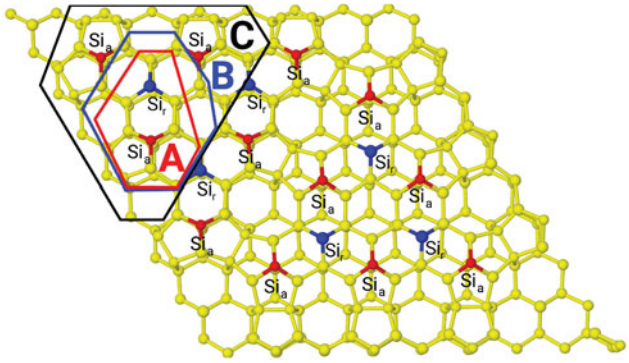

Figure 1. The two top double layers of the Si(111)-7×7 surface unit cell taken from Ref. [37]: The faulted half is in the upper left and the unfaulted in the lower right. Rest-atoms and adatoms are marked with Si_r and Si_a, respectively. The outermost lines indicate cuts done to obtain cluster **C**, the next lines the cuts for **B** and the inner lines for **A** (see Figure 2).

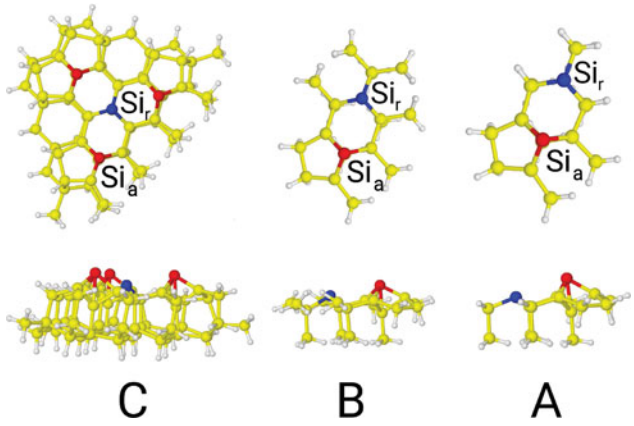

Figure 2. The three clusters **A**, **B**, **C** investigated in this study with the hydrogen atoms (white) used to saturate broken Si–Si bonds viewed from top (along the surface normal, upper figures) and the side (parallel to the surface plane, lower figures). Again, rest-atoms (Si_r) are coloured blue, adatoms (Si_a) red and all other Si-atoms yellow.

from a DFT slab structure taken from Ref. [37] with a unit cell consisting of 498 atoms in 12 layers arranged in the so-called dimer-adatom-stacking fault structure [38]. The two top double layers of the unit cell are shown in Figure 1. The unit cell can be divided in a faulted (upper left) and an unfaulted half (lower right). Each half contains six so-called adatoms, Si_a, and three rest-atoms, Si_r.

The red, blue and black lines in Figure 1 indicate the cuts taken to build our model clusters of different size. We chose an adsorption site on the faulted half at a centre adatom and rest-atom position as the core of our model clusters. This adsorption site showed the highest reaction rates in previous experimental studies [28] and was therefore chosen to be investigated. We chose the same protocol for construction of the clusters as in Ref. [34]. All Si–Si bonds cut, in order to obtain the clusters, were saturated with hydrogen atoms. In order to keep the local electronic structure at the Si-atoms involved in the chemisorption as similar as possible compared to the periodic surface, the hydrogens were put such, that the direction of the H-Si bond is exactly the same as the one for the Si–Si bond in the infinite surface. The Si-H bond length was set to 1.51 Å and then the Cartesian positions of the hydrogen atoms used to saturate the clusters are kept fixed in all calculations. All other degrees of freedom are fully optimised in the calculations reported here, if not stated otherwise.

The minimum requirement for a cluster used to model different degrees of charge localisation in the quantum chemistry calculations is that the cluster gives similar results regarding chemisorption geometries and energies in the neutral state as the large ones used in Ref. [25]. Therefore, we demand a deviation of less than 20 % of the binding energy as a quantitative measure and that no difference in the qualitative energetic preference for specific adsorbate orientations should occur.

The smallest cluster we found, which fulfills the requirement stated above, is **A** shown on the right in Figure 2 together with **B** (middle) and **C** (left). Note that cluster **B** is the same as the small cluster and **C** as the large one in Ref. [34]. Cluster **A** consists of 17 silicon atoms saturated with 26 hydrogen atoms. Apart from a centre adatom and the neighbouring rest-atom also all Si atoms directly bound to them and selected silicon atoms with 'two bonds' distance are included. The surrounding of the adatom needs to include more atoms than the one of the rest-atom, reflecting its bigger role in the chemisorption and the probable desorption mechanisms (see below). Cluster **B** consists of 21 silicon atoms saturated by 34 hydrogen atoms. Here in addition to the atoms included in cluster **A,** all silicon atoms with 'two bonds' distance to the centre adatom and the neighbouring rest-atom are included. Finally, the largest cluster, **C**, consists of 67 silicon atoms, which are saturated by 54 hydrogen atoms. It includes a corner adatom and two centre adatoms as well as a central rest-atom. This cluster is already so large, that its charged states are markedly different to the ones of the small clusters (see Section 3) and thus is used to represent delocalised or 'free' surface charges in what follows and in Ref. [34]. We also constructed and tested several additional clusters with both smaller and larger numbers of atoms. However, smaller clusters failed to describe chemisorption. Bigger clusters delivered no additional substantial information while demanding higher computational costs. Clusters including more than one adatom or rest-atom fail to describe charge localisation in our approach appropriately. In such clusters no relevant

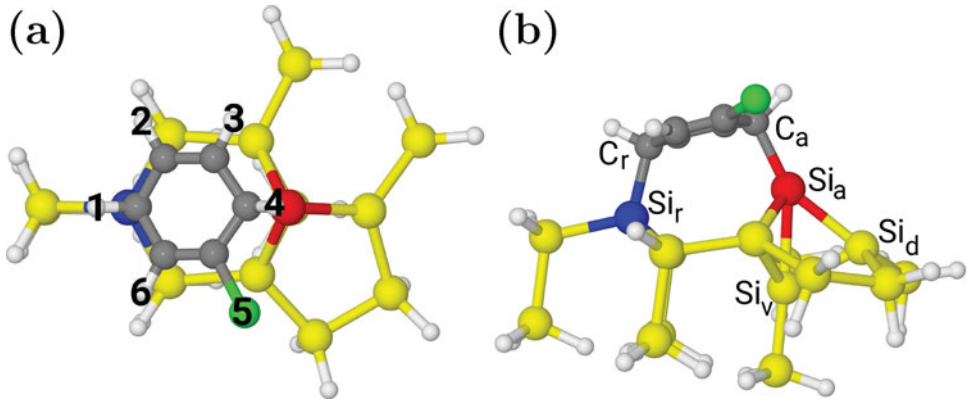

Figure 3. (a) Numbering scheme of possible Cl-positions for chlorobenzene on the clusters. Here, Cl-position 5 is shown for cluster **A**-PhCl, in top view. (b) Labelling of selected atoms shown for cluster **A**-PhCl, shown in side view. For the atoms the same colours are used as in Figure 2, the chlorine atom in position 5 is green and the carbon atoms grey.

couplings to nuclear degrees of freedom, which could lead to desorption, were found. However, such couplings are a requirement for a resonance model to describe the STM-induced desorption (see below). Also, other functionals, such as M06, M062X, PBE0, CAM-B3LYP and BP86 were tested, but no relevant differences were found [39–43]. For a recent general assessment of the performance of DFT functionals see Refs. [44,45].

2.2. Quantum chemistry

We used the B3LYP [46] hybrid functional with different basis sets up to quadruple zeta quality together with the Grimme D3 dispersion correction [47] in Ref. [25]. With this methodology, we could successfully model the chemisorption and physisorption for neutral clusters and publish a value for the chemisorption energy, which differed significantly from theoretical and experimental results at that time. However, this value was later confirmed by new experiments within an error margin of ≈0.2 eV (see above). The results further indicated that a double zeta basis set is sufficient to describe the system and yields reasonable adsorption energies if counterpoise corrections (CPC) [48] are done. Therefore, we decided to use the B3LYP functional as implemented in Gaussian09 [49] together with the less demanding 6-31G* [50] basis set in Ref. [34], which yields comparable chemisorption energies for the large cluster, i.e. 1.598 eV for B3LYP-D3/def2-TZVP as implemented in the TURBOMOLE program package [51] in Ref. [25] compared to 1.639 eV for B3LYP/6-31G* for cluster **C** [34] (both values with CPC applied). With the 6-31G* basis set, we get counterpoise corrections in a small range between ≈0.20 and ≈0.25 eV for the chemisorbed systems, nearly independent on the functional and the chemisorption minimum. Therefore, we will report energies without CPC for simplicity in the following.

The small clusters, **A** and **B**, are also able to describe the chemisorption on the B3LYP-D3/6-31G* level of theory and yield chemisorption energies of 1.681 eV for cluster **A** and of 1.675 eV for cluster **B** compared with 1.875 eV for cluster **C** (all values without CPC). We use PBE [52] in combination with density fitting – again with D3 and a 6-31G* basis set within Gaussian09 – as a second density functional approach, which yields quite comparable chemisorption energies in the neutral state. The values for PBE-D3/6-31G* are 1.722 eV (**A**), 1.725 eV (**B**) and 1.831 eV (**C**). Note, for both DFT approaches Cl-position 3 is slightly (≈7 meV) more stable than Cl-position 5 for clusters **A** and **B**, see Figures 3(a) and 4. However, for cluster **C** Cl-position 5 is the most preferred one (19 meV lower in energy for B3LYP-D3 and 6 meV for PBE-D3). If

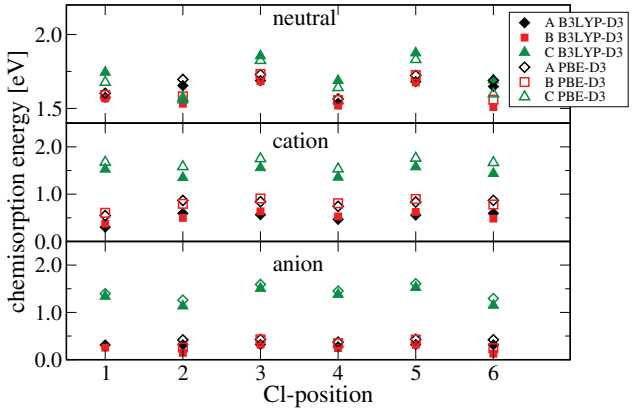

Figure 4. The binding energies for chlorobenzene are shown for the neutral (top), anionic (middle) and cationic species (bottom) for different positions of the chlorine atom (see Figure 3(a)). Results for **A**-PhCl are given as black diamonds, for **B**-PhCl as red squares and for **C**-PhCl as green triangles. B3LYP-D3 results are indicated by filled symbols, PBE-D3 results by non-filled ones (all values without CPC).

not stated otherwise, we always refer to Cl-position 5, as we take cluster **C** as the reference for the infinite surface. However, most properties are fairly independent on the Cl-position (see below).

The electrostatic potential derived charges (ESP-charges) given below were calculated according to the Merz–Singh–Kollman scheme [53,54].

3. Results

3.1. Energies

We calculated the chemisorption energies for all six possible orientations of the chlorine atom in the di-σ bonded structure on the clusters (see Figure 3(a) for cluster **A**). The binding energies for the chemisorption are shown in Figure 4 for the neutral clusters (top graph), the cationic clusters (middle graph) and the anionic clusters (lower graph). Energies for PhCl chemisorbed on **A** (**A**-PhCl) are indicated by black diamonds, the ones for PhCl chemisorbed on **B** (**B**-PhCl) as red squares, and for PhCl chemisorbed on **C** (**C**-PhCl) as green triangles. B3LYP-D3 results are indicated by filled symbols, PBE-D3 results by non-filled ones. As one can see, for the neutral clusters all three cluster show very similar energies with differences up to ≈0.15 eV and also qualitatively the same trends for both B3LYP+D3 and PBE+D3. Cl-positions 3 and 5, i.e. ortho to the carbon atom bound to the adatom, are the most stable ones and have nearly the same energy. As already mentioned, for **A**-PhCl and **B**-PhCl Cl-position 3 is the most stable one and for **C**-PhCl Cl-position 5. Cl-positions 5 will be used for the investigations in what follows, if not stated otherwise.

In the middle and lower graphs of Figure 4, one can see that the situation is quite different for the charged systems. Here, we see a large reduction of the binding energies for the small clusters, while the energies for the large cluster are not strongly affected. We attribute these changes to the fact, that the small cluster size restricts the excess charge to regions near to the chemisorption site and thus models a localised or 'confined' charge on the surface, which may otherwise only be observed in a very costly dynamical approach for the bigger clusters. Similar approaches have been used for local STM-manipulations, for instance benzene on Si(001) by Seideman and co-workers [17]. As one can see, the main findings for these localised charges are rather independent on the details of the cluster for the chemisorption energy, i.e. there are not many differences between **A**-PhCl and **B**-PhCl, and the different functionals, i.e. B3LYP-D3 and PBE-D3, yield comparable results. The only qualitative difference occurs for Cl-position 1, where no stable geometry on the PB3-D3 level of theory could be found for **A**-PhCl$^-$ and **B**-PhCl$^-$. Here, all optimisations led to a dissociation of the carbon chlorine bond.

Table 1. Given are vertical ionisation potentials (IPs) and electron affinities (EAs) calculated in a Δ-SCF procedure for the clean clusters and the chemisorbed systems on the PBE-D3 and B3LYP-D3 level of theory. All values are in eV.

	PBE-D3		B3LYP-D3	
	IP	EA	IP	EA
A	5.88	2.82	5.95	2.76
B	6.21	2.99	6.13	2.96
C	5.26	3.59	5.08	3.74
A-PhCl	6.85	1.28	7.10	1.14
B-PhCl	6.71	1.63	7.12	1.36
C-PhCl	5.43	3.30	5.21	3.54

3.2. Electron affinities and ionisation potentials

As already stated, we use the charged clusters to model a coherent superposition of excited states of a charged extended system. In this approach, we have no direct access to the excitation energy of the resonance, which we try to simulate. As in Ref. [34], we use the following estimate as an indirect measure: we calculate electron affinities (EAs) and ionisation potentials (IPs) for the extended system (here represented by **C**) and for the small clusters (**A** and **B**). The differences between these energies are then taken as a rough measure for the energy needed to form the localised ion resonance. We computed vertical IPs and EAs for the clean clusters, i.e. clusters with no chlorobenzene attached, and clusters with a chemisorbed chlorobenzene for B3LYP-D3 and PBE-D3 using a Δ-SCF procedure. The results are given in Table 1. Here, vertical means that the optimised geometry of the neutral state was considered and no geometrical relaxation was taken into account. One can see that the IPs and EAs derived from PBE-D3 are very similar to those computed with B3LYP-D3 (differences always smaller than 0.3 eV). Such similarities between a pure density functional and a hybrid functional have also been reported for organic acceptor molecules recently [55].

For B3LYP-D3, we see that the IP is about 1 eV larger for the small clean clusters, **A** and **B**, and about 1.9 eV for the small clusters with chlorobenzene adsorbed, **A**-PhCl and **B**-PhCl, compared with the large clusters **C** and **C**-PhCl. This means a 'confined' hole in the charged clusters **A** or **B** has ≈1.5 eV excess energy compared to a 'free' hole in cluster **C**. Although, the results for PBE-D3 are quite similar with respect to absolute numbers, we get only a difference of 0.62 eV between **C** and **A**, which hints to the fact, that the determined excess energies can only be regarded as rough estimates. Furthermore, one sees that **A** and **B** have about 1.0 and 0.8 eV smaller EAs than **C**

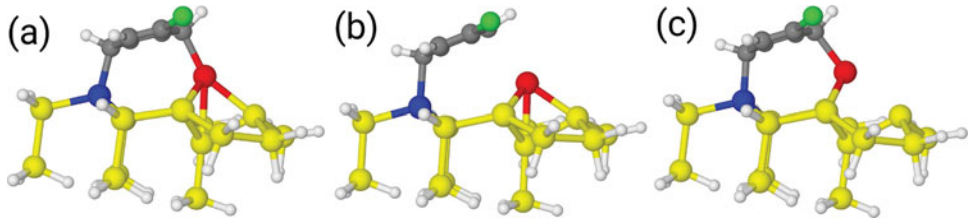

Figure 5. Optimised geometries for the neutral (a), cationic (b) and anionic (c) species of **A**-PhCl obtained form the B3LYP-D3/6-31G* calculations. The same colour code is used as in Figure 3.

and that **A**-PhCl and **B**-PhCl have 2.4 and 2.2 eV smaller EAs compared with **C**-PhCl for the B3LYP-D3 results. In the PBE-D3 case, these numbers are in the same order of magnitude, i.e. 0.8 eV (**A**) and 0.6 eV (**B**) for the clean systems and 2.0 eV (**A**-PhCl) and 1.7 eV (**B**-PhCl) for the chemisorbed systems.

Although these numbers are only rough estimates, they nevertheless indicate, that the charged clusters could be at least a reasonable model for localised 'hot' charge carriers with an excess energy in the range of the experimentally observed thresholds, i.e. bias voltages of 1.4 V (electrons) [29] and -1.2 V (holes) [30]. Nevertheless, the estimated energies seem to be more sensitive to the choice of the cluster and/or the quantum chemistry method than most other quantities (see below).

3.3. Geometries

Geometry optimisation was performed for all charge states, in order to assess the influence of the charge localisation on the nuclear coordinates for all clusters with and without chlorobenzene adsorbed. Such optimised geometries for **A**-PhCl at the B3LYP-D3/6-31G* level of theory are given in Figure 5. One can see that the most striking geometrical changes occur with participation of the adatom.

The values of selected bond lengths and their changes upon charging are shown in Table 2 for the clean clusters and in Table 3 for the chemisorbed systems. The labelling of the respective atoms is given in Figure 3(b). Again there are no qualitative differences between PBE-D3 and B3LYP-D3. Generally, the observed changes upon charging are a bit more pronounced for B3LYP-D3 than for PBE-D3. For the clean clusters in the neutral and the cationic state most values are quite comparable. The only exception is the distance between the adatom, Si_a, the underlying silicon atom, Si_v, i.e. $R_{Si_a-Si_v}$. We attribute this to the fact that the exact shape of the trigonal bipyramidal arrangement of silicon atoms depends very delicately on the details of the surrounding in the clusters. For the small clusters, this arrangement is horizontally compressed, which leads to comparable $R_{Si_a-Si_d}$ but different $R_{Si_a-Si_v}$. It is the other way round, i.e. $R_{Si_a-Si_v}$ is comparable while $R_{Si_a-Si_d}$ is a bit shorter in **C**-PhCl, in case of the clusters with chlorobenzene adsorbed (see Table 3). However, many properties, like for instance binding energies (see above), are mostly unaffected by these effects.

Table 2. Selected bond lengths for the clean clusters in the neutral systems and their changes, Δ, in charged systems. All values are given in Å. For the labelling of the atoms see Figure 3(b). Most significant changes are in boldface.

	PBE-D3		B3LYP-D3	
	$R_{Si_a-Si_d}$	$R_{Si_a-Si_v}$	$R_{Si_a-Si_d}$	$R_{Si_a-Si_v}$
A	2.461	2.471	2.446	2.418
Δ**A**$^+$	− 0.032	− 0.046	− 0.012	0.009
Δ**A**$^-$	0.044	**0.181**	0.071	**0.255**
B	2.446	2.430	2.443	2.418
Δ**B**$^+$	− 0.011	− 0.006	0.010	0.011
Δ**B**$^-$	0.059	**0.222**	0.073	**0.262**
C	2.432	2.840	2.425	2.770
Δ**C**$^+$	− 0.013	− 0.037	− 0.009	0.032
Δ**C**$^-$	− 0.011	− 0.054	0.004	0.018

While all clean clusters show only little changes in the selected bond length in the cationic state, $R_{Si_a-Si_v}$ and to a lesser extent $R_{Si_a-Si_d}$ are substantially elongated in the anionic state of the small clusters. The same can be found for the anionic small cluster with chlorobenzene where also $R_{Si_a-Si_v}$ and $R_{Si_a-Si_d}$ are changed while the Si-C bond lengths, i.e. $R_{Si_r-C_r}$ and $R_{Si_a-C_a}$, are much less affected. This means for the 'confined' electrons mainly the adatom geometry is changed, which can also be seen in Figure 5(c). In contrast, for the 'confined' hole the main effect is seen for the bond between the adatom and the respective carbon atom (see Figure 5(b)). Consequently one finds large changes in $R_{Si_a-C_a}$ for the cationic small clusters with chlorobenzene. For the large cluster, i.e. the 'free' charges, only small bond length changes are seen for all cases.

For B3LYP-D3 the main changes in the geometries, i.e. the elongation of $R_{Si_a-C_a}$ for the cation and the elevation of Si_a in the anion, are fairly independent on the Cl-position. For instance, we get changes for $R_{Si_a-C_a}$ between 0.885 Å (Cl-position 3) and 1.182 Å (Cl-position 4) in **A**-PhCl$^+$ for all possible Cl-positions shown in Figure 3(a).

Table 3. Selected bond lengths in the neutral adsorbate covered systems and their changes, Δ, in charged systems. All values are given in Å. For the labelling of the atoms see Figure 3(b). Most significant changes are in boldface.

	PBE-D3				B3LYP-D3			
	$R_{Si_r-C_r}$	$R_{Si_a-C_a}$	$R_{Si_a-Si_d}$	$R_{Si_a-Si_v}$	$R_{Si_r-C_r}$	$R_{Si_a-C_a}$	$R_{Si_a-Si_d}$	$R_{Si_a-Si_v}$
A-PhCl	2.027	2.055	2.587	2.716	2.018	2.035	2.619	2.728
Δ**A**-PhCl$^+$	0.086	**0.725**	− 0.091	− 0.176	0.087	**0.889**	− 0.116	− 0.185
Δ**A**-PhCl$^-$	0.020	0.049	**0.326**	**0.201**	− 0.025	0.042	**0.391**	**0.226**
B-PhCl	2.028	2.053	2.596	2.722	2.018	2.034	2.627	2.734
Δ**B**-PhCl$^+$	0.083	**0.774**	− 0.102	− 0.181	0.091	**0.927**	− 0.125	− 0.189
Δ**B**-PhCl$^-$	− 0.023	0.056	**0.319**	**0.206**	− 0.028	0.041	**0.397**	**0.232**
C-PhCl	2.024	2.005	2.420	2.799	2.016	1.992	2.427	2.791
Δ**C**-PhCl$^+$	− 0.003	0.000	0.001	0.005	− 0.004	0.001	0.000	0.006
Δ**C**-PhCl$^-$	0.004	0.001	0.002	− 0.004	0.005	0.000	0.001	− 0.003

We find 0.920 Å (Cl-position 3) and 1.218 Å (Cl-position 4) as maximal and minimal changes in **B**-PhCl$^+$. One gets changes in $R_{Si_a-Si_v}$ in the range of 0.214 Å (Cl-position 1) to 0.238 Å (Cl-position 4) for **A**-PhCl$^-$, and 0.216 Å (Cl-position 1) to 0.244 Å (Cl-position 4) for **B**-PhCl$^-$ in the anion calculated with B3LYP-D3.

The situation is similar in the case of PBE-D3. Here, we observe changes of $R_{Si_a-C_a}$ for **A**-PhCl$^+$ in between 0.720 Å (Cl-position 3) and 1.097 Å (Cl-position 4). For **B**-PhCl$^+$, we get values between 0.666 Å (Cl-position 6) and 1.149 Å (Cl-position 4). As already stated above, there is no stable chemisorption geometry for Cl-position 1 for PBE-D3 in the anion. The situation is again comparable to B3LYP-D3 for all other Cl-positions. We find changes of $R_{Si_a-Si_v}$ for **A**-PhCl$^-$ in a range from 0.197 Å (Cl-position 2) to 0.204 Å (Cl-position 4), for **B**-PhCl$^-$ in between 0.195 Å (Cl-position 4) and 0.206 Å (Cl-position 5).

3.4. Charge localisation

As a next step, we computed ESP-charges for the different chemisorbed systems. All calculations were done for optimised geometries in the respective charge states and we always refer to atomic charges with hydrogens summed into heavy atoms. We found that – especially for the large systems – the ESP-charges show a slight dependence on the used coordinate system. Therefore, the `NoSymm` keyword was used in all calculations, in order to keep the coordinate system defined by the Cartesian coordinates of the fixed hydrogen atoms, which are determined through the underlying unit cell structure.

We first investigated, where the additional charge is located, i.e. in the cluster or on the molecule. Therefore, we computed the sums of ESP-charges for the cluster atoms and for the chlorobenzene atoms. These sums and the differences upon charging are given in Table 4. For all systems in the neutral state there is a charge transfer from the cluster to the molecule. Here, **B**-PhCl and **C**-PhCl show a much larger charge transfer (≈0.2 e) than **A**-PhCl (≈0.07 e).

Table 4. Sum of ESP-charges with hydrogens summed into heavy atoms for the chlorobenzene molecule (adsorbate) and the different clusters for neutral systems. For the anions and cations the differences, Δ, to the neutral system are given.

	PBE-D3		B3LYP-D3	
	Adsorbate	Cluster	Adsorbate	Cluster
A-PhCl	− 0.059	0.059	− 0.076	0.076
Δ**A**-PhCl$^-$	− 0.127	− 0.873	− 0.089	− 0.911
Δ**A**-PhCl$^+$	0.301	0.699	0.295	0.705
B-PhCl	− 0.170	0.170	− 0.213	0.213
Δ**B**-PhCl$^-$	− 0.091	− 0.909	− 0.063	− 0.937
Δ**B**-PhCl$^+$	0.264	0.736	0.286	0.714
C-PhCl	− 0.261	0.261	− 0.286	0.286
Δ**C**-PhCl$^-$	− 0.032	− 0.968	− 0.030	− 0.970
Δ**C**-PhCl$^+$	0.048	0.952	0.030	0.970

One sees that the additional charge mainly goes to the cluster atoms for the sum of charges of the anions. Here, only −0.089 e (**A**-PhCl$^-$), −0.063 e (**B**-PhCl$^-$) and −0.03 e (**C**-PhCl$^-$) of the additional negative charge end up on the molecule for the B3LYP-D3 calculations. Again, PBE-D3 yields similar results (i.e. −0.127 , −0.091 and −0.032 e).

For the large cationic cluster, **C**-PhCl$^+$, the situation is comparable and again only 0.03 e of the additional charge goes to the molecule for B3LYP-D3 and 0.048 e for PBE-D3. In contrast, the additional positive charge is much more concentrated on the molecule for the small clusters. One finds 0.295 e for **A**-PhCl$^+$ and 0.286 e for **B**-PhCl$^+$ as a change in the sum of charges for B3LYP-D3. For PBE-D3, 0.301 e (**A**-PhCl$^+$) and 0.264 e (**B**-PhCl$^+$) are observed.

The computed charge localisations, or more precisely their changes, nicely correspond to the geometric changes, for the confined charge carriers. In both cases we see for the electrons large changes in the cluster at the adatom. For holes the molecule and the molecule adatom bond are mostly affected. These changes are fairly

Table 5. Atom resolved ESP charges with hydrogens summed into heavy atoms for **A**-PhCl, **B**-PhCl and **C**-PhCl. For the anions and cations differences, Δ, to the neutral systems are given. Labels are explained for the case of **A**-PhCl in Figure 3(b). The most significant differences are in boldface.

	PBE-D3			B3LYP-D3		
	Si_a	Si_d	C_a	Si_a	Si_d	C_a
A-PhCl	0.075	−0.066	−0.111	0.074	−0.075	−0.092
Δ**A**-PhCl$^+$	−0.089	0.108	**0.556**	−0.087	0.121	**0.543**
Δ**A**-PhCl$^-$	**−0.172**	**−0.173**	0.059	**−0.216**	**−0.202**	0.041
B-PhCl	0.149	−0.063	−0.278	0.149	−0.073	−0.258
Δ**B**-PhCl$^+$	−0.105	0.082	**0.502**	−0.097	0.065	**0.623**
Δ**B**-PhCl$^-$	**−0.162**	**−0.200**	0.003	**−0.200**	**−0.225**	0.069
C-PhCl	0.104	−0.004	−0.053	0.119	−0.021	−0.058
Δ**C**-PhCl$^+$	−0.008	0.004	0.107	0.032	0.004	0.029
Δ**C**-PhCl$^-$	−0.033	−0.008	−0.030	−0.012	−0.007	−0.047

independent on details of the small cluster, although the absolute values of atomic charges differ more than expected between **A**-PhCl and **B**-PhCl.

Furthermore, these changes are fairly independent on the Cl-position. For instance, we get changes in the range between −0.028 e (Cl-position 2) and −0.109 e (Cl-position 1) for the adsorbate charge in **A**-PhCl$^-$ and between −0.026 e (Cl-position 4) and −0.066 e (Cl-position 1) in **B**-PhCl$^-$ for B3LYP-D3. For the cations, we find changes of the adsorbate charge from 0.258 e (Cl-position 1) to 0.422 e (Cl-position 4) in **A**-PhCl$^+$ and form 0.268 e (Cl-position 6) to 0.444 e (Cl-position 4) in **B**-PhCl$^+$, again for the B3LYP-D3 case.

The individual charges of the cluster and adsorbate atoms are given for selected atoms in Table 5 for B3LYP-D3 and PBE-D3 for Cl-position 5. One sees that the positive charge on the adsorbate is mainly located on the C-atom bound to the adatom in the neutral chemisorption geometry (C_a) and that the negative charge is on Si_a (adatom) and Si_d for the case of the small clusters (**A**-PhCl and **B**-PhCl). For the large cluster (**C**-PhCl) the changes in these charges are negligible. This hints to rather delocalised charges in the case of the large cluster. Again, the B3LYP-D3 and the PBE-D3 results agree very well.

3.5. Frequencies

In Ref. [34], we demonstrated that the low-temperature activation energies for non-local desorption [33] either induced by electrons, (13 ± 3) meV, or holes, (60 ± 10) meV, can be understood in terms of normal modes of cluster **B**-PhCl on the B3LYP-D3/6-31G* level of theory. Normal modes were calculated, for which the mass of the fixed saturating hydrogens was set to 10^{15} amu (1.66×10^{-12}kg). Furthermore, the linear transit coordinates between optimised neutral geometry and the geometries of the charged systems are projected on the normal coordinates (see, for instance Ref. [56]). However, an identification of the most important modes only by the projection coefficients turned out to be misleading, because of the normalisation, which implicitly contains the mass of the moving atoms. Furthermore, the linear transit paths are rather large amplitude motions, which are not well described by only a few normal modes. Therefore, we related the normal modes in the respective energy ranges with substantial projection coefficients to the geometric changes described above, i.e. the $R_{Si_a-C_a}$ elongation and the adatom elevation. For **B**-PhCl with B3LYP-D3 we identified two modes in Ref. [34], one at at 500.0 cm^{-1} (61.99 meV) with a large $Si_a - C_a$ stretch and one at 96.5 cm^{-1} (11.96 meV), which represented an

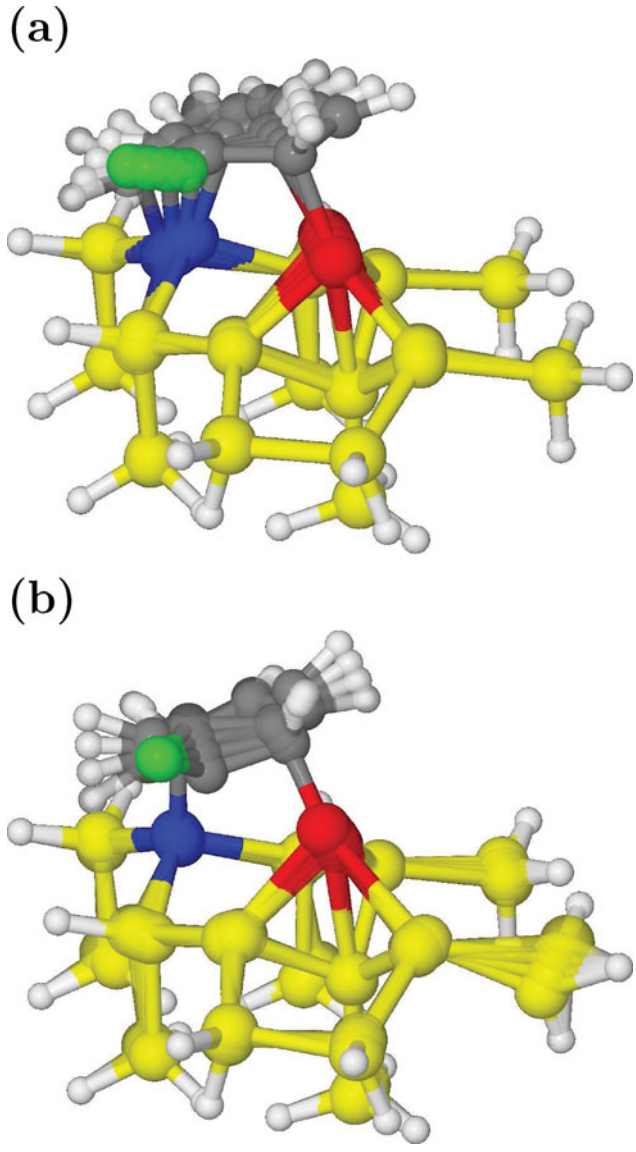

Figure 6. Overlays with increasing opacity along selected normal coordinates, which have large contributions to the linear transit paths towards the optimised geometry of the charged states of **A**-PhCl calculated on the B3LYP-D3/6-31G* level of theory: (a) a mode at 498.3 cm^{-1} (61.8 meV) with a large $Si_a - C_a$ stretch contribution, (b) a mode at 96.6 cm^{-1} (12.3 meV), representing the adatom elevation.

adatom elevation. Here, we assume that a displacement along the normal coordinates pointing to the geometry of the charged state will lower the energy difference between neutral and charged state and lead to a higher probability of forming the resonance state.

In order to proof the robustness of these results, we do the same analysis also for **A**-PhCl and for both functionals, B3LYP-D3 and PBE-D3. The resulting modes for **A**-PhCl calculated with B3LYP-D3 are sketched in Figure 6. These modes have energies of (a) 498.3 cm^{-1} (61.8 meV) and (b) 99.6 cm^{-1} (12.3 meV). For PBE-D3 we get similar results, however, most frequencies are a bit smaller. For the $Si_a - C_a$ stretch in the anionic case, we find two important modes for **A**-PhCl at 480.2 cm^{-1} (59.5 meV) and 482.9 cm^{-1} (59.9 meV) and one mode at 447.5 cm^{-1} (55.4 meV) for **B**-PhCl. The adatom wagging is mainly described by a mode with 59.8 cm^{-1} (7.41 meV) for **A**-PhCl and a mode with 57.8 cm^{-1} (7.17 meV) for **B**-PhCl. These energies are slightly outside the experimental error bars but still in the right order of magnitude. Such differences are not completely unexpected, as normal mode analysis for such low frequency modes are known to be rather unreliable.

4. Conclusions and outlook

We reported a comparison between two different small clusters for the simulation of hot localised charge carriers on the Si(111)-7×7 surface. Many findings of this model approach, which uses small clusters to approximate a superposition of charged states of the extended surface, seem to be rather independent on the details of the clusters used and the underlying quantum chemistry method. For instance, the localisation of the excess charge and the induced geometry changes are nearly independent on the used functional and cluster. Also, the identification of normal modes promoting desorption was possible for all approaches within or near to the energy range matching experimental low-temperature activation energies. However, other properties as the estimates of the resonance energies or the absolute atomic charges are more sensitive to details of the model. Therefore, we plan to validate the approach for other benzene derivates and perform first steps towards a dynamical description of the desorption process, i.e. by Born–Oppenheimer molecular dynamics. Especially for such computationally demanding simulations at finite temperatures, it is important to use clusters as small as possible.

Acknowledgment

We thank R.E. Palmer and S. Holmes for very fruitful and enjoyable discussions and the Deutsche Forschungsgemeinschaft for financial support through grant KL-1387/3-1.

Disclosure statement

No potential conflict of interest was reported by the authors.

Funding

Deutsche Forschungsgemeinschaft [grant number KL-1387/3-1].

ORCID

Manuel Utecht http://orcid.org/0000-0002-6677-0775

References

[1] J.A. Stroscio and D.M. Eigler, Science **254**(5036), 1319–1326 (1991). doi:10.1126/science.254.5036.1319
[2] I.W. Lyo and P. Avouris, Science **253**(5016), 173–176 (1991). doi:10.1126/science.253.5016.173
[3] L. Bartels, G. Meyer, and K.H. Rieder, Phys. Rev. Lett. **79**(4), 697–700 (1997). doi:10.1103/PhysRevLett.79.697
[4] W. Ho, J. Chem. Phys. **117**(24), 11033–11061 (2002). doi:10.1063/1.1521153
[5] K. Maeda and K. Domen, J. Phys. Chem. Lett. **1**(18), 2655–2661 (2010). doi:10.1021/jz1007966
[6] B. Boudaïffa, P. Cloutier, D. Hunting, M.A. Huels, and L. Sanche, Science **287**(5458), 1658–1660 (2000). doi:10.1126/science.287.5458.1658
[7] S. Sakulsermsuk, P.A. Sloan, and R.E. Palmer, ACS Nano **4**, 7344 (2010). doi:10.1021/nn101468e
[8] P.A. Sloan, S. Sakulsermsuk, and R.E. Palmer, Phys. Rev. Lett. **105**, 048301 (2010). doi:10.1103/PhysRevLett.105.048301
[9] J.R. Hahn and W. Ho, Phys. Rev. Lett. **87**, 166102 (2001). doi:10.1103/PhysRevLett.87.166102
[10] X.H. Qiu, G.V. Nazin, and W. Ho, Phys. Rev. Lett. **93**, 196806 (2004). doi:10.1103/PhysRevLett.93.196806
[11] P. Liljeroth, J. Repp, and G. Meyer, Science **317**(5842), 1203–1206 (2007). doi:10.1126/science.1144366
[12] C. Nacci, J. Lagoute, X. Liu, and S. Fölsch, Phys. Rev. B **77**(12), 121405(R) (2008). doi:10.1103/PhysRevB.77.121405
[13] B.N.J. Persson and J.E. Demuth, Solid State Commun. **57**, 769–772 (1986). doi:10.1016/0038-1098(86)90856-2
[14] B.N.J. Persson and A. Baratoff, Phys. Rev. Lett. **59**, 339–342 (1987). doi:10.1103/PhysRevLett.59.339
[15] C. Nacci, S. Fölsch, K. Zenichowski, J. Dokić, T. Klamroth, and P. Saalfrank, Nano Lett. **9**(8), 2996–3000 (2009). doi:10.1021/nl901419g
[16] K. Zenichowski, J. Dokić, T. Klamroth, and P. Saalfrank, J. Chem. Phys. **136**, 094705 (2012). doi:10.1063/1.3692229
[17] S. Alavi, R. Rousseau, S.N. Patitsas, G.P. Lopinski, R.A. Wolkow, and T. Seideman, Phys. Rev. Lett. **85**, 5372–5375 (2000). doi:10.1103/PhysRevLett.85.5372
[18] A. Abe, K. Yamashita, and P. Saalfrank, Phys. Rev. B **67**, 235411 (2003). doi:10.1103/PhysRevB.67.235411
[19] K. Zenichowski, C. Nacci, S. Fölsch, J. Dokić, T. Klamroth, and K. Saalfrank, J. Phys.: Condens. Matter **24**, 394009 (2012). doi:10.1088/0953-8984/24/39/394009
[20] P. Avouris and R.E. Walkup, Annu. Rev. Phys. Chem. **40**(1), 173–206 (1989). doi:10.1146/annurev.pc.40.100189.001133

[21] J.A. Misewich, T.F. Heinz, and D.M. Newns, Phys. Rev. Lett. **68**, 3737–3740 (1992). doi:10.1103/PhysRevLett.68.3737
[22] P.A. Sloan, M.F.G. Hedouin, R.E. Palmer, and M. Persson, Phys. Rev. Lett. **91**, 118301 (2003). doi:10.1103/PhysRevLett.91.118301
[23] P.H. Lu, J.C. Polanyi, and D. Rogers, J. Chem. Phys. **111**(22), 9905–9907 (1999). doi:10.1063/1.480325
[24] T.L. Pan, P.A. Sloan, and R.E. Palmer, Chem. Rec. **14**(5), 841–847 (2014). doi:10.1002/tcr.201402021
[25] M. Utecht, T. Pan, T. Klamroth, and R.E. Palmer, J Phys. Chem. A **118**(33), 6699–6704 (2014). doi:10.1021/jp504208d
[26] Y. Cao, J.F. Deng, and G.Q. Xu, J. Chem. Phys. **112**(10), 4759–4767 (2000). doi:10.1063/1.481032
[27] X. Chen, Q. Kong, J. Polanyi, D. Rogers, and S. So, Surf. Sci. **340**(3), 224–230 (1995). doi:10.1016/0039-6028(95)00732-6
[28] D. Lock, S. Sakulsermsuk, R.E. Palmer, and P.A. Sloan, J. Phys.: Condens. Matter **27**(5), 054003 (2015). doi:10.1088/0953-8984/27/5/054003
[29] D. Lock, K.R. Rusimova, T.L. Pan, R.E. Palmer, and P.A. Sloan, Nat. Commun. **6**, 8365 (2015). doi:10.1038/ncomms9365
[30] K.R. Rusimova, N. Bannister, P. Harrison, D. Lock, S. Crampin, R.E. Palmer, and P.A. Sloan, Nat. Commun. **7**, 12839 (2016). doi:10.1038/ncomms12839
[31] K.R. Rusimova and P.A. Sloan, Nanotechnology **28**(5), 054002 (2017). doi:10.1088/1361-6528/28/5/054002
[32] T.L. Pan, P.A. Sloan, and R.E. Palmer, J. Phys. Chem. Lett. **5**(20), 3551–3554 (2014). doi:10.1021/jz501819n
[33] S.A. Holmes, CONTROL AND MANIPULATION OF SMALL MOLECULES IN THE SCANNING TUNNELING MICROSCOPE thesis submitted to The University of Birmingham for the degree of DOCTOR OF PHILOSOPHY, 2017.
[34] M. Utecht, R.E. Palmer, and T. Klamroth, Phys. Rev. Mater. **1**, 026001 (2017). doi:10.1103/PhysRevMaterials.1.026001
[35] L. Mitas, J.C. Grossman, I. Stich, and J. Tobik, Phys. Rev. Lett. **84**, 1479–1482 (2000). doi:10.1103/PhysRevLett.84.1479
[36] J.L. Gavartin, P.V. Sushko, and A.L. Shluger, Phys. Rev. B **67**, 035108 (2003). doi:10.1103/PhysRevB.67.035108
[37] J. Ciston, A. Subramanian, I.K. Robinson, and L.D. Marks, Phys. Rev. B **79**, 193302 (2009). doi:10.1103/PhysRevB.79.193302
[38] K. Takayanagi, Y. Tanishiro, M. Takahashi, and S. Takahashi, J. Vac. Sci. Technol. A **3**, 1502–1506 (1985). doi:10.1116/1.573160
[39] J.P. Perdew, Phys. Rev. B **33**(12), 8822–8824 (1986). doi:10.1103/PhysRevB.33.8822
[40] A.D. Becke, Phys. Rev. A **38**(6), 3098–3100 (1988). doi:10.1103/PhysRevA.38.3098
[41] T. Yanai, D.P. Tew, and N.C. Handy, Chem. Phys. Lett. **393**(1–3), 51–57 (2004). doi:10.1016/j.cplett.2004.06.011
[42] C. Adamo and V. Barone, J. Chem. Phys. **110**(13), 6158–6170 (1999). doi:10.1063/1.478522
[43] Y. Zhao and D.G. Truhlar, Theor. Chem. Acc. **120**(1–3), 215–241 (2008). doi:10.1007/s00214-007-0310-x
[44] N. Mardirossian and M. Head-Gordon, Mol. Phys. **115**(19), 2315–2372 (2017). doi:10.1080/00268976.2017.1333644
[45] L. Goerigk, A. Hansen, C.A. Bauer, S. Ehrlich, A. Najibi, and S. Grimme, Phys. Chem. Chem. Phys. **115**(19), 32184–32215 (2017). doi:10.1039/C7CP04913G
[46] A.D. Becke, J. Chem. Phys. **98**, 5648 (1993). doi:10.1063/1.464913
[47] S. Grimme, J. Antony, S. Ehrlich, and H. Krieg, J. Chem. Phys. **132**, 154104 (2010). doi:10.1063/1.3382344
[48] S.F. Boys and F. Bernardi, Mol. Phys. **19**, 553 (1970). doi:10.1080/00268977000101561
[49] M.J. Frisch, G.W. Trucks, H.B. Schlegel, G.E. Scuseria, M.A. Robb, J.R. Cheeseman, G. Scalmani, V. Barone, B. Mennucci, G.A. Petersson, H. Nakatsuji, M. Caricato, X. Li, H.P. Hratchian, A.F. Izmaylov, J. Bloino, G. Zheng, J.L. Sonnenberg, M. Hada, M. Ehara, K. Toyota, R. Fukuda, J. Hasegawa, M. Ishida, T. Nakajima, Y. Honda, O. Kitao, H. Nakai, T. Vreven, J.A. Montgomery, Jr., J.E. Peralta, F. Ogliaro, M. Bearpark, J.J. Heyd, E. Brothers, K.N. Kudin, V.N. Staroverov, R. Kobayashi, J. Normand, K. Raghavachari, A. Rendell, J.C. Burant, S.S. Iyengar, J. Tomasi, M. Cossi, N. Rega, J.M. Millam, M. Klene, J.E. Knox, J.B. Cross, V. Bakken, C. Adamo, J. Jaramillo, R. Gomperts, R.E. Stratmann, O. Yazyev, A.J. Austin, R. Cammi, C. Pomelli, J.W. Ochterski, R.L. Martin, K. Morokuma, V.G. Zakrzewski, G.A. Voth, P. Salvador, J.J. Dannenberg, S. Dapprich, A.D. Daniels, Ã. Farkas, J.B. Foresman, J.V. Ortiz, J. Cioslowski, and D.J. Fox, Gaussian'09 Revision D.01 (Gaussian Inc., Wallingford, CT, 2013).
[50] P.C. Hariharan and J.A. Pople, Theor. Chim. Acta **28**, 213 (1973). doi:10.1007/BF00533485
[51] TURBOMOLE V6.5 2013, a development of University of Karlsruhe and Forschungszentrum Karlsruhe GmbH, 1989-2007, TURBOMOLE GmbH, since 2007; available from http://www.turbomole.com.
[52] J.P. Perdew, K. Burke, and M. Ernzerhof, Phys. Rev. Lett. **77**, 3865–3868 (1996). doi:10.1103/PhysRevLett.77.3865
[53] B.H. Besler, K.M. Merz, Jr., and P.A. Kollman, J. Comp. Chem. **11**, 431 (1990). doi:10.1002/jcc.540110404
[54] U.C. Singh and P.A. Kollman, J. Comp. Chem **5**, 129 (1984). doi:10.1002/jcc.540050204
[55] L. Gallandi, N. Marom, P. Rinke, and T. Körzdörfer, J. Chem. Theory. Comput. **12**(2), 605–614 (2016). doi:10.1021/acs.jctc.5b00873
[56] T. Klamroth, J. Chem. Phys. **124**(14), 144310 (2006). doi:10.1063/1.2185633